

Duality Models: An Embarrassingly Simple One-step Generation Paradigm

Peng Sun^{1,2} Xinyi Shang^{3,4} Tao Lin¹ Zhiqiang Shen⁴

Abstract

Consistency-based generative models like Shortcut and MeanFlow achieve impressive results via a target-aware design for solving the Probability Flow ODE (PF-ODE). Typically, such methods introduce a target time r alongside the current time t to modulate outputs between a local multi-step derivative ($r = t$) and a global few-step integral ($r = 0$). However, the conventional “one input, one output” paradigm enforces a partition of the training budget, often allocating a significant portion (e.g., 75% in MeanFlow) solely to the multi-step objective for stability. This separation forces a trade-off: allocating sufficient samples to the multi-step objective leaves the few-step generation undertrained, which harms convergence and limits scalability.

To this end, we propose **Duality Models (DUMO)** via a “one input, dual output” paradigm. Using a shared backbone with dual heads, DUMO simultaneously predicts velocity \mathbf{v}_t and flow-map \mathbf{u}_t from a single input \mathbf{x}_t . This applies geometric constraints from the multi-step objective to every sample, bounding the few-step estimation without separating training objectives, thereby significantly improving stability and efficiency. On ImageNet 256×256 , a 679M Diffusion Transformer with SD-VAE achieves a state-of-the-art (SOTA) **FID of 1.79 in just 2 steps**. Code is available at: <https://github.com/LINs-lab/DuMo>.

1. Introduction

Diffusion probabilistic models have fundamentally transformed the landscape of generative Artificial Intelligence, demonstrating unprecedented capability in high-fidelity image synthesis and distribution modeling (Ho et al., 2020;

¹Westlake University, Hangzhou, China ²Zhejiang University, Hangzhou, China ³University College London, London, UK ⁴Mohamed bin Zayed University of Artificial Intelligence, Abu Dhabi, UAE. Correspondence to: Tao Lin <lin-tao@westlake.edu.cn>.

Preprint. February 23, 2026.

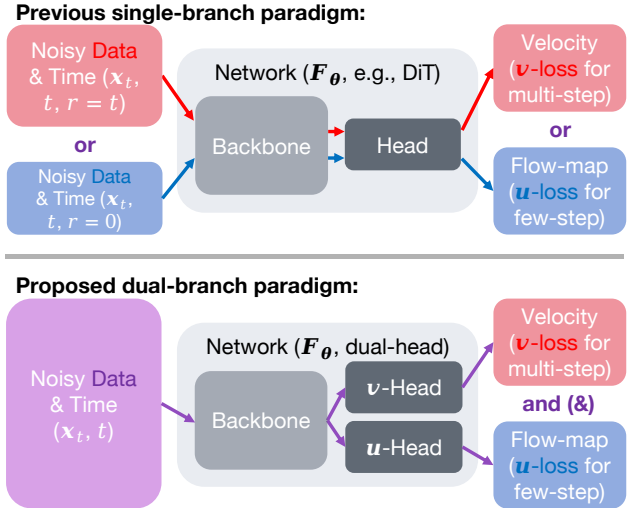


Figure 1. **Schematic comparison.** (Top) Existing one-step models (Geng et al., 2025; Cheng et al., 2025) adopt a “one input, one output” scheme, predicting either velocity \mathbf{v}_t or flow-map \mathbf{u}_t conditioned on r . (Bottom) DUMO employs a “one input, dual output” design to simultaneously predict \mathbf{v}_t and \mathbf{u}_t from \mathbf{x}_t . This incurs negligible overhead ($< 0.5\%$, e.g., +3M on a 675M DiT) by adding only an output head while preserving the backbone.

Song et al., 2020). Despite their success, the standard formulation requires solving the PF-ODE through dozens or hundreds of iterative steps, creating a significant computational bottleneck during inference. To mitigate this latency, the community has actively explored acceleration techniques, with *consistency-based methods* (Song et al., 2023) emerging as a premier paradigm for mapping noise to data in as few as one or two steps.

However, scaling consistency-based methods to large-scale, high-resolution models remains a formidable challenge due to their notorious training instability (Sun & Lin, 2026; Cheng et al., 2025). Without sufficient local constraints, the recursive enforcement of self-consistency often leads to optimization divergence or mode collapse. To counteract this volatility, recent SOTA approaches, such as Shortcut (Frans et al., 2024), MeanFlow (Geng et al., 2025) and RCGM (Sun & Lin, 2026), have adopted a *target-aware* design. These methods introduce a target time r to modulate the learning objective: the model minimizes a stable multi-step regression loss (velocity field) when $r \approx t$, and switches to the volatile few-step consistency loss (flow-map) only when

$r = 0$. By anchoring the training process in the stable velocity field, these methods prevent divergence, enabling consistency training to scale to complex datasets.

While effective for stability, we contend that this “one input, one output” paradigm imposes a **structural bottleneck on the generation quality**. Since the network is constrained to predict *either* the velocity *or* the flow-map for any given input, the training process necessitates a trade-off in data partitioning. To prevent divergence, existing methods are compelled to route the vast majority of training samples (e.g., up to 75% in MeanFlow (Geng et al., 2025)) exclusively to the auxiliary velocity task. Crucially, this leaves the flow-map head—which is solely responsible for inference—effectively “**starved**” of supervision. This severe data scarcity does not merely slow down convergence: it **fundamentally caps the performance ceiling**, trapping the one-step generator in a suboptimal regime despite the large-scale pre-training (Geng et al., 2025; Frans et al., 2024; Lu & Song, 2024). Moreover, this issue becomes particularly acute when training large-scale models on massive datasets (Sun & Lin, 2026; Cheng et al., 2025).

In this paper, we propose to resolve this trade-off via a novel **Duality Models** (DUMO) framework. Breaking away from the conditional switching paradigm, DUMO employs a simple yet effective “one input, dual output” architecture that simultaneously predicts both the local velocity \mathbf{v}_t and the global flow-map \mathbf{u}_t from a single noisy input \mathbf{x}_t . This design is mathematically elegant: it allows the geometric constraints of the PF-ODE (provided by the velocity head) to act as a regularizer for the flow-map prediction on *every single training sample*, without the need to partition the training data budget. By jointly optimizing these objectives in a single model with dual heads, DUMO inherently bridges the gap between stability and data efficiency.

Our contributions are summarized as follows:

- (a) We identify a critical bottleneck in existing target-aware models: the requisite partition of the training budget creates a data scarcity for the generative objective, limiting the performance ceiling of one-step sampling.
- (b) We propose DUMO, a “one input, dual output” framework that unifies the learning of velocity and flow-maps. This design leverages multi-step physics to bound and regularize few-step estimation on every sample, ensuring both stability and efficiency.
- (c) We achieve SOTA performance on ImageNet 256×256 . DUMO enables a 679M-parameter Diffusion Transformer with SD-VAE to reach an FID of 1.79 in just 2 sampling steps, surpassing previous teacher-free methods in both convergence speed and generation quality.

We detail our *remarkably simple and effective* framework DUMO in [Alg. 1](#). Notably, DUMO does *not* require complex

parameter design, specialized loss functions, or learning curricula to stabilize training and scaling, as justified by our comprehensive empirical validation in [Sec. 4](#).

2. Background and Preliminaries

Generative modeling via diffusion aims to learn a mapping from a simple prior distribution $p_1(\mathbf{z}) = \mathcal{N}(\mathbf{0}, \mathbf{I})$ to a complex data distribution $p_0(\mathbf{x})$. Modern continuous-time generative models, including Diffusion Models (Ho et al., 2020; Song et al., 2020) and Flow Matching (FM) (Lipman et al., 2022), unify this process through the lens of the PF-ODE.

Consider a probability path $p_t(\mathbf{x})$ interpolating between data at $t = 0$ and noise at $t = 1$. A sample \mathbf{x}_t along this path is typically constructed via an affine transformation of data $\mathbf{x} \sim p_0$ and noise $\mathbf{z} \sim p_1$:

$$\mathbf{x}_t = \alpha(t)\mathbf{z} + \gamma(t)\mathbf{x}, \quad (1)$$

where $\alpha(t), \gamma(t) \in C^1[0, 1]$ are schedule functions satisfying boundary conditions $\alpha(0) = 0, \gamma(0) = 1$ (pure data) and $\alpha(1) = 1, \gamma(1) = 0$ (pure noise). The trajectory of samples over time defines a vector field $\mathbf{v}_t(\mathbf{x}_t)$, which characterizes the instantaneous velocity of the probability mass transport. The corresponding PF-ODE is given by:

$$\frac{d\mathbf{x}_t}{dt} = \mathbf{v}_t(\mathbf{x}_t), \quad \text{where } \mathbf{v}_t(\mathbf{x}_t) \text{ is the velocity field.} \quad (2)$$

Generative sampling is performed by numerically integrating (2) from $t = 1$ to $t = 0$. Depending on the learning target relative to this ODE, existing methods can be broadly categorized into two paradigms: learning the local derivative (Multi-step) or learning the global integral (Few-step).

2.1. Multi-step Models: Learning the Local Derivative

Diffusion and Flow-matching models focus on learning the local geometry of the PF-ODE. Specifically, they aim to approximate the velocity field \mathbf{v}_t defined in (2). As unified in previous studies (Sun et al., 2025; Lipman et al., 2022), despite differences in transport paths, the core objective is to regress a neural network $\mathbf{v}_\theta(\mathbf{x}_t, t)$ to the ground-truth conditional velocity field. The general loss function is:

$$\mathcal{L}_v(\theta) = \mathbb{E}_{t, \mathbf{x}, \mathbf{z}} \left[\|\mathbf{v}_\theta(\mathbf{x}_t, t) - \dot{\mathbf{x}}_t\|_2^2 \right], \quad (3)$$

where $\dot{\mathbf{x}}_t = \frac{d}{dt}(\alpha(t)\mathbf{z} + \gamma(t)\mathbf{x})$ represents the target velocity derived from the forward process. A conceptual illustration of this learning paradigm is provided in [Fig. 2\(a\)](#).

Remarks. This paradigm relies on a simple regression objective (ℓ_2 loss) to a stable target. Consequently, training is notoriously stable and scalable. However, sampling requires solving the ODE with small step sizes to faithfully follow the local curvature, necessitating dozens or hundreds of function evaluations (NFE), which hinders real-time applications.

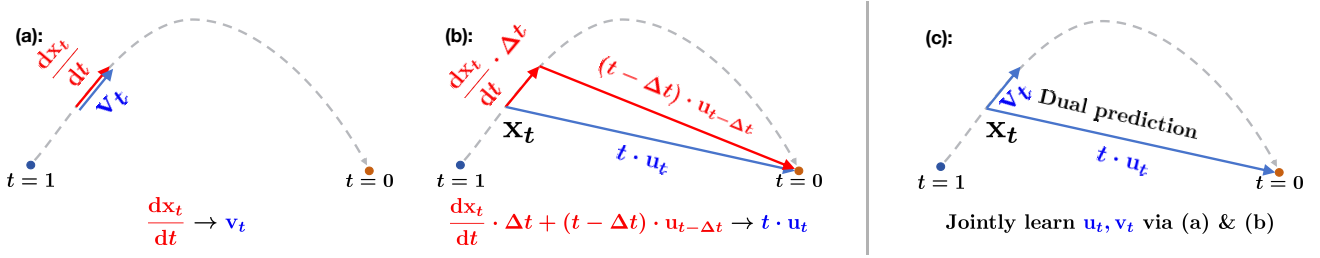


Figure 2. **Conceptual illustration of learning paradigms.** Trajectories illustrate the mapping from a **current prediction state** to a **target learning state**. (a) Multi-step methods, such as standard diffusion (Ho et al., 2020) and flow-matching (Lipman et al., 2022), learn the local derivative (velocity). (b) Prominent one-step approaches, including consistency models (Song et al., 2023), MeanFlow (Geng et al., 2025), and Shortcut models (Frans et al., 2024), learn the global integral (flow-map). (c) DUMO unifies these paradigms via a dual-output architecture, establishing a natural combination of the geometric constraints from (a) and the generative efficiency of (b).

2.2. Consistency-based Few-step Models

To accelerate sampling, Consistency Models (Song et al., 2023) and Flow-map models (Geng et al., 2025; Frans et al., 2024) learn the PF-ODE integral directly. Unlike local derivative methods (v_t), these approaches parameterize a *global flow-map* $u_\theta(x_t, t)$. Here, $t \cdot u_\theta(x_t, t)$ represents a straight-line vector from x_t to the data x_0 .

The **self-consistency principle** behind consistency models states that points on the same ODE trajectory must map to the same origin. Consistency models enforce this by ensuring predictions at t and $t - \Delta t$ remain consistent:

$$t \cdot u_\theta(x_t, t) \equiv \frac{dx_t}{dt} \cdot \Delta t + (t - \Delta t) u_\theta(x_{t-\Delta t}, t). \quad (4)$$

Training uses a recursive objective where the model learns from its own predictions (bootstrapping) rather than fixed ground truth. Recent methods (Frans et al., 2024; Geng et al., 2025; Sun & Lin, 2026) introduce a target time r to modulate between local and global predictions; see Fig. 2(b).

Remarks. By approximating the integral mapping, these models facilitate 1-step or few-step generation. However, training stability is often compromised by the recursive nature of the objective (i.e., the “moving target” problem) and the difficulty of learning the global flow without local constraints. Consequently, these methods often require complex training schedules or large batch sizes, presenting a trade-off between training stability and sampling efficiency.

3. Methodology

In this section, we present DUMO, a framework designed to overcome the structural limitations of existing target-aware generative models. We begin by analyzing the dilemma inherent in the single-branch paradigm, identifying a critical trade-off between training stability and sample efficiency (Sec. 3.1). Building on this analysis, we introduce our **Dual-Branch** design, which unifies the learning of local velocity and global flow-maps to resolve this conflict

(Sec. 3.2). Finally, we detail the practical implementation of our framework, including the architectural modifications and the training algorithm (Sec. 3.3 and Alg. 1).

3.1. Revisiting the Dilemma in Single-Branch Paradigm

Modern SOTA one-step generative models, such as MeanFlow (Geng et al., 2025) and Shortcut models (Frans et al., 2024), predominantly adopt a *single-branch paradigm* coupled with a mixture optimization strategy. Formally, these methods can be viewed as optimizing a composite objective governed by a hyperparameter ρ (the Velocity Ratio):

$$\mathcal{L}(\theta) = \mathbb{E}_{x,z,t,p} [\mathbb{I}_{p < \rho} \cdot \underbrace{\mathcal{L}_v(\theta)}_{\text{Stability}} + \mathbb{I}_{p \geq \rho} \cdot \underbrace{\mathcal{L}_u(\theta)}_{\text{Efficacy}}], \quad (5)$$

where $p \sim \text{Uniform}(0, 1)$ is a random variable determining the task for the current step, and $\mathcal{L}_v, \mathcal{L}_u$ denote the multi-step (velocity) and few-step (flow-map) losses, respectively, as defined in Sec. 2. This formulation creates a **zero-sum trade-off** between two critical requirements:

- Training stability:** The velocity loss \mathcal{L}_v is indispensable for grounding the generation process in the physical constraints of the PF-ODE. As evidenced in prior studies (Sun et al., 2025; Geng et al., 2025; Sun & Lin, 2026; Cheng et al., 2025), this term provides stable, low-variance supervision. We illustrate this empirically in Fig. 3: removing this supervision ($\rho = 0.0$) leads to training divergence (high MMD). Consequently, existing methods are forced to allocate a dominant portion of the training budget (e.g., $\rho \in [0.75, 0.9]$) solely to stabilize the optimization (Geng et al., 2025).
- Few-step generation efficacy:** Conversely, the capability for one-step generation stems directly from \mathcal{L}_u . However, the high ρ required for stability inevitably limits the effective training data for this objective. As shown in Fig. 3, while a balanced ratio improves results, an excessive focus on stability ($\rho = 1.0$) fails to optimize the flow-map effectively, thus significantly degrading generation quality.

In practice, this dilemma forces a compromise: models

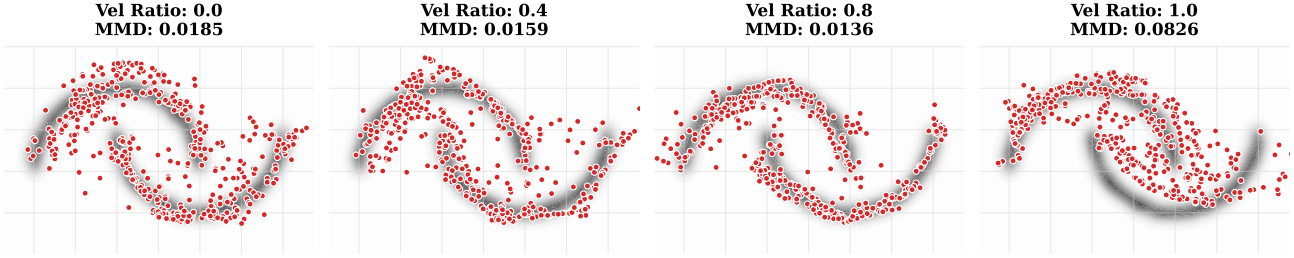


Figure 3. **Impact of Velocity Ratio (ρ) on one-step generation using MeanFlow (Geng et al., 2025).** We visualize samples generated on the Moons dataset to analyze the behavior of this representative single-branch model. Gray areas: Ground truth distribution; Red dots: Samples generated via one-step inference. We report Maximum Mean Discrepancy (MMD) to quantify quality (lower is better). The results highlight a rigid trade-off: low velocity supervision ($\rho = 0$) leads to instability/divergence, while excessive supervision ($\rho = 1.0$) hampers the learning of the few-step mapping. Optimal performance is achieved at $\rho = 0.8$, confirming that MeanFlow requires a specific partition of the training budget to balance stability and efficacy.

must sacrifice data efficiency to prevent divergence. The root cause lies in the **single-branch constraint**: the network is structurally incapable of leveraging the geometric stability of the ODE derivative to regularize the flow-map prediction within a single forward pass. This observation motivates our proposed Dual-Branch design, which aims to dissolve this trade-off by simultaneously satisfying both objectives.

3.2. Key Design of Dual-Branch Paradigm

In this section, we elaborate on the architectural design of DUMO and justify its efficacy. Without loss of generality, we anchor our exposition in the “Linear” transport path (i.e., $\alpha(t) = t, \gamma(t) = 1 - t$), a setting widely adopted in recent one-step generative models (Frans et al., 2024; Geng et al., 2025; Sun & Lin, 2026; Sun et al., 2025; Cheng et al., 2025).

Dual-branch diffusion and flow models. Conventional single-branch diffusion and flow-matching models typically parameterize a network $F_\theta(\mathbf{x}_t, t)$ to approximate the velocity field alone (Sun et al., 2025; Ho et al., 2020). In contrast, we propose a *dual-branch* formulation where the model simultaneously predicts two distinct geometric quantities:

$$F_\theta(\mathbf{x}_t, t) = (\mathbf{v}_{\theta,t}, \mathbf{u}_{\theta,t}), \quad (6)$$

which aim to learn the instantaneous velocity $\mathbf{v}_t := \frac{d\mathbf{x}_t}{dt}$ and the flow-map $\mathbf{u}_t := \frac{\mathbf{x}_t - \mathbf{x}_0}{t}$ targeting the data endpoint \mathbf{x}_0 along the PF-ODE trajectory passing through \mathbf{x}_t .

Dual loss design in DUMO. Leveraging this simultaneous prediction capability, we construct a composite objective that unifies local geometric constraints with global consistency enforcement. For the velocity head, we adopt the standard flow-matching regression loss:

$$\mathcal{L}_v(\theta) = \mathbb{E}_{\mathbf{x}_0, \mathbf{z}, t} \left[\|\mathbf{v}_{\theta,t} - \mathbf{v}_t\|_2^2 \right], \quad (7)$$

where the target velocity is given by $\mathbf{v}_t = \mathbf{z} - \mathbf{x}_0$ under the linear path. For the flow-map head, we employ the

consistency training objective (Song et al., 2023; Lu & Song, 2024; Geng et al., 2025; Sun & Lin, 2026):

$$\mathcal{L}_u(\theta) = \mathbb{E}_{\mathbf{x}_0, \mathbf{z}, t} \left[\left\| \mathbf{u}_{\theta,t} - \mathbf{v}_t + t \cdot \frac{d\mathbf{u}_{\theta^-,t}}{dt} \right\|_2^2 \right], \quad (8)$$

where θ^- denotes a copy of the parameters with stopped gradients (or a target network). The total training objective is a weighted combination of these two terms:

$$\mathcal{L}(\theta) = \beta \cdot \mathcal{L}_v(\theta) + (1 - \beta) \cdot \mathcal{L}_u(\theta). \quad (9)$$

A conceptual illustration of this learning paradigm is provided in Fig. 2(c). Intuitively, the hyperparameter β governs the trade-off between *training stability*—inherent to the velocity regression \mathcal{L}_v —and *generation efficiency*, which is driven by the consistency objective \mathcal{L}_u . We provide a detailed analysis of β and its empirical settings in Sec. 4.

Justification on compatibility. For (9), one might question whether combining velocity and flow-map losses creates conflicting gradients, as these tasks are conventionally treated separately. In App. D, we analyze and justify the compatibility of these objectives, demonstrating that they are theoretically consistent within our framework.

3.3. Practical Design Implementation

This section details implementation strategies ensuring the stability and efficiency of DUMO. We cover time sampling, guidance integration, loss function selection, and architectural modifications for the dual-head paradigm.

Time distribution sampling. To align the training process with the signal-to-noise ratio of the data, we adopt a flexible time sampling strategy, following established practices (Frans et al., 2024; Sun et al., 2025; Sun & Lin, 2026; Song et al., 2023). Specifically, time steps are sampled as $t \sim \text{Beta}(\theta_1, \theta_2)$. The hyperparameters θ_1 and θ_2 allow us to bias the training focus towards specific noise levels

(e.g., concentrating on mid-trajectory regions where consistency learning is most critical). We provide detailed ablation studies on the choice of θ_1 and θ_2 in [Sec. 4.4](#).

Enhanced target velocity via guidance. It is well-established that incorporating guidance during training or sampling significantly improves perceptual quality (Ho & Salimans, 2022; Dhariwal & Nichol, 2021; Karras et al., 2022). Theoretically, this corresponds to modifying the conditional target score function from $\nabla_{\mathbf{x}_t} \log p_t(\mathbf{x}_t)$ to an enhanced version $\nabla_{\mathbf{x}_t} \log \left(p_t(\mathbf{x}_t|\mathbf{c}) \cdot \left(\frac{p_{t,\theta}(\mathbf{x}_t|\mathbf{c})}{p_{t,\theta}(\mathbf{x}_t|\emptyset)} \right)^\zeta \right)$, where $\zeta \in (0, 1)$ denotes the enhancement ratio (guidance scale).

In practice, we implement this via *Training-time Classifier-Free Guidance* (CFG). We update the ground-truth velocity target \mathbf{v}_t used in (7) and (8) using the model’s own predictions: $\mathbf{v}_t \leftarrow \mathbf{v}_t + \zeta \cdot (\mathbf{v}_{\theta^-,t} - \mathbf{v}_{\theta^-,t,\emptyset})$, where $\mathbf{v}_{\theta^-,t,\emptyset}$ represents the unconditional prediction from the EMA (or stop-gradient) model. This aligns our implementation with recent SOTA frameworks (Frans et al., 2024; Geng et al., 2025; Sun et al., 2025; Sun & Lin, 2026).

Simplicity in loss design. While the standard ℓ_2 -norm is ubiquitous in multi-step diffusion training (Ho et al., 2020), few-step distillation methods often require complex, task-specific loss functions (e.g., LPIPS or heavily weighted ℓ_2 variants) to prevent signal decay (Song & Dhariwal, 2023; Geng et al., 2025). These specialized losses introduce additional hyperparameters (e.g., norm orders p) that necessitate extensive tuning for different resolutions or architectures. *In contrast, we demonstrate the **robustness and simplicity** of DUMO by utilizing the standard, unweighted ℓ_2 -norm for all experiments. Our method achieves SOTA results without relying on complex metric engineering.*

Efficient u-loss calculation. The consistency loss term in (8) involves a time derivative $\frac{d\mathbf{u}_{\theta^-,t}}{dt}$, which technically requires a Jacobian-vector product (JVP) computation (Lu & Song, 2024). To mitigate the computational overhead of JVP, we adopt the efficient JVP-free approximation proposed in Sun et al. (2025). This method utilizes a central finite-difference approximation to estimate the tangent vector, reducing the cost to simple forward passes without auto-differentiation through the graph.

Architectural adaptation for dual heads. We adapt standard single-head architectures (e.g., Diffusion Transformers (Peebles & Xie, 2023)) to the DUMO paradigm with minimal structural changes. We retain the entire backbone encoder and simply introduce a parallel output projection layer (head) for the flow-map \mathbf{u}_t , while the original head continues to predict \mathbf{v}_t . The parameter overhead is negligible; for instance, adding a second head to a 675M parameter DiT in-

Algorithm 1. DUMO Training Step

Require: Data distribution $p(\mathbf{x})$, model parameters θ , stop gradient operator **sg**, enhancement ratio ζ , Beta distribution parameters (θ_1, θ_2) , loss weighting factor β .

- 1: **Preparation Phase:**
- 2: Sample data $\mathbf{x} \sim p(\mathbf{x})$ and noise $\mathbf{z} \sim \mathcal{N}(\mathbf{0}, \mathbf{I})$.
- 3: Sample time step $t \sim \text{Beta}(\theta_1, \theta_2)$.
- 4: Construct perturbed state $\mathbf{x}_t = t \cdot \mathbf{z} + (1 - t) \cdot \mathbf{x}$.
- 5: Compute ground truth velocity $\mathbf{v}_t = \mathbf{z} - \mathbf{x}$.
- 6: **Learning Target Estimation:**
- 7: Compute model outputs $(\mathbf{v}_{\theta,t}, \mathbf{u}_{\theta,t}) = \mathbf{F}_\theta(\mathbf{x}_t, t)$.
- 8: Compute unconditional prediction $\mathbf{v}_{\theta^-,t,\emptyset}$.
- 9: Enhance velocity: $\mathbf{v}_t \leftarrow \mathbf{v}_t + \zeta \cdot (\mathbf{sg}(\mathbf{v}_{\theta,t}) - \mathbf{v}_{\theta^-,t,\emptyset})$.
- 10: Compute flow-map target: $\mathbf{u}_t = \mathbf{v}_t - t \cdot \frac{d\mathbf{u}_{\theta^-,t}}{dt}$.
- 11: **Loss Calculation & Model Update:**
- 12: Update parameters θ by minimizing the objective:

$$\mathcal{L}(\theta) = \beta \cdot \|\mathbf{v}_{\theta,t} - \mathbf{v}_t\|_2^2 + (1 - \beta) \cdot \|\mathbf{u}_{\theta,t} - \mathbf{u}_t\|_2^2$$

creases the model size by only $\sim 3\text{M}$ parameters ($< 0.5\%$).

Computational efficiency. [Alg. 1](#) summarizes the complete training procedure of DUMO. A key advantage is that simultaneous prediction of $\mathbf{v}_{\theta,t}$ and $\mathbf{u}_{\theta,t}$ eliminates redundant forward passes during target enhancement. Specifically, when computing the enhanced target velocity $\mathbf{v}_t \leftarrow \mathbf{v}_t + \zeta \cdot (\mathbf{v}_{\theta^-,t} - \mathbf{v}_{\theta^-,t,\emptyset})$, standard methods require a separate forward pass to obtain $\mathbf{v}_{\theta,t}$. In our framework, this term is already available from the main forward pass (detached via `stopgrad`), eliminating redundant computation.

*DUMO achieves superior computational efficiency. Each training step requires only **1 gradient-tracking** and **3 gradient-free** forward passes. In comparison, SOTA single-branch methods like MeanFlow (Geng et al., 2025) (using JVP-free implementations) require **1 gradient-tracking** and **4 gradient-free** passes, making DUMO approximately **12% more efficient** per iteration (cf., [Sec. 4.4](#) for more details).*

4. Experiments

We empirically validate the DUMO framework. We first detail the experimental setup, covering datasets, architectures, and training protocols, followed by an evaluation of generation quality and efficiency against SOTA baselines.

4.1. Experimental Setup

Datasets and latent space operations. We conduct our primary evaluation on the ImageNet-1K dataset (Deng et al., 2009) at resolutions of 256×256 and 512×512 , adhering to established benchmarks in high-fidelity generative mod-

eling (Karras et al., 2024; Song et al., 2023). We follow the standard preprocessing pipeline from ADM (Dhariwal & Nichol, 2021). To ensure computational efficiency, all experiments are performed in the latent space:

- (a) 256×256 : We utilize the widely adopted SD-VAE (Rombach et al., 2022) as the default autoencoder.
- (b) 512×512 : In addition to SD-VAE, we employ DC-AE (Chen et al., 2024a), which offers a higher compression ratio ($f32c32$), to mitigate the computational demands of high-resolution training.

Network architectures. We adopt the Diffusion Transformer (DiT) (Peebles & Xie, 2023) as our backbone, consistent with recent SOTA few-step generation methods (Frans et al., 2024; Geng et al., 2025; Sun et al., 2025). Specifically, we use the DiT-XL/2 variant (675M parameters). To adapt this single-branch architecture for our DUMO paradigm, we introduce a parallel output head for flow-map prediction (\mathbf{u}_t) alongside the original velocity head (\mathbf{v}_t). Crucially, this modification incurs a negligible parameter overhead of approximately 3M ($< 0.5\%$ increase), preserving the model’s computational efficiency.

Implementation details. Models are implemented in PyTorch (Paszke, 2019) and trained using the AdamW optimizer (Loshchilov & Hutter, 2017) with $\beta_1 = 0.9, \beta_2 = 0.95$, and no weight decay. We use a constant learning rate of 1×10^{-4} and a global batch size of 512. Further hyperparameter configurations are analyzed and detailed in Sec. 4.4 and App. C.1. Evaluation is performed using the standard Fréchet Inception Distance (FID) (Heusel et al., 2017), computed on 50,000 generated samples against the full training set, following the protocol of Ho et al. (2020).

4.2. Comparison with SOTA Few-step Methods

As presented in Tab. 1, we primarily compare our DUMO with **teacher-free single-branch models**. Unlike distillation-based approaches that rely on pre-trained teacher networks, these methods (including ours) learn the generation trajectory directly. We demonstrate that our dual-branch design significantly enhances the efficiency and quality of this direct training paradigm.

Comparison on 512×512 resolution. Under the standard training schedule (360 epochs), our dual-branch paradigm proves more effective than the conventional single-branch design. We achieve an FID of **2.76**, surpassing MeanFlow-XL/4 (3.41 FID) by a clear margin. Notably, even when compared to the parameter-heavy sCT-XXL (1.5B params), our method yields superior results while being significantly more compact. When equipped with the DC-AE, our performance improves to **2.23** FID. This result is particularly impressive as it outperforms sCD-M (2.26 FID)—a distillation-

based model—demonstrating that our teacher-free approach can rival the quality of distilled models without their associated pipeline complexity.

Comparison on 256×256 resolution. The superiority of our dual-branch paradigm is further pronounced in the long-training regime. DUMO achieves FID **1.79** with 2 NFEs, establishing a new SOTA for teacher-free models. We substantially outperform single-branch baselines such as MeanFlow-XL/2 (2.20 FID) and the computationally demanding IMM-XL/2 (3.99 FID, 3840 epochs). This indicates that the bottleneck in direct consistency training lies not in the training duration, but in the paradigm itself, which our dual-branch formulation effectively resolves.

Summary. DUMO sets a new benchmark among Teacher-free One-step Models. By addressing the limitations of single-branch paradigm, it consistently outperforms strong baselines like MeanFlow and sCT, offering the best trade-off between generation quality and training simplicity.

4.3. Exploration of Higher-Order Multiplicity

A natural question arises: *given the efficacy of dual-branch learning, does extending the framework to predict additional geometric quantities (i.e., scaling beyond two output heads) yield further gains?* We investigate this “Multiplicity Model” hypothesis on ImageNet-1K 256×256 by equipping the backbone with **three** output heads. We evaluate two representative configurations trained for 424 epochs:

- (a) **Tri-head (FM + MeanFlow + Consistency):** Simultaneously predicts velocity, the MeanFlow target (Geng et al., 2025), and the consistency mapping. The 1-NFE FID degrades to 2.84 (vs. 2.60 FID for our dual-branch baseline).
- (b) **Tri-head (FM + Shortcut + Consistency):** Predicts velocity, the Shortcut target (Frans et al., 2024), and consistency. Performance drops to an FID of 4.73.

We attribute these negative results to two primary factors:

- (a) **Homologous redundancy:** Theoretically, Flow Matching, MeanFlow, and Shortcut are all derived from the same underlying PF-ODE mechanics (Sun et al., 2025; Sun & Lin, 2026). Consequently, they provide highly correlated supervision signals. Adding a third branch offers marginal information gain while merely increasing the optimization complexity.
- (b) **Quality of supervision:** As observed in Tab. 1, baselines like Shortcut exhibit relatively poor intrinsic performance (FID > 10.0). Including such objectives acts as a “noisy teacher”, introducing suboptimal gradients that effectively drag down the overall training trajectory.

Conclusion: The dual-branch design appears to be the optimal “sweet spot” within the PF-ODE paradigm. To

Duality Models

Table 1. System-level quality comparison for few-step generation task on class-conditional ImageNet-1K. The best results of each resolution are highlighted. Notation $A \oplus B$ denotes the result obtained by combining methods A and B.

512 × 512					256 × 256				
Method	NFE ↓	FID ↓	#Params	#Epochs	Method	NFE ↓	FID ↓	#Params	#Epochs
Diffusion & flow-matching models									
ADM-G (Dhariwal & Nichol, 2021)	250×2	7.72	559M	388	ADM-G (Dhariwal & Nichol, 2021)	250×2	4.59	559M	396
U-ViT-H/4 (Bao et al., 2023)	50×2	4.05	501M	400	U-ViT-H/2 (Bao et al., 2023)	50×2	2.29	501M	400
DiT-XL/2 (Peebles & Xie, 2023)	250×2	3.04	675M	600	DiT-XL/2 (Peebles & Xie, 2023)	250×2	2.27	675M	1400
SiT-XL/2 (Ma et al., 2024)	250×2	2.62	675M	600	SiT-XL/2 (Ma et al., 2024)	250×2	2.06	675M	1400
MaskDiT (Zheng et al., 2023)	79×2	2.50	736M	-	DDT-XL/2 (Wang et al., 2025)	250×2	1.26	675M	400
EDM2-S (Karras et al., 2024)	63	2.56	280M	1678	REPA-XL/2 (Yu et al., 2024)	250×2	1.96	675M	200
EDM2-L (Karras et al., 2024)	63	2.06	778M	1476	REPA-XL/2 (Yu et al., 2024)	250×2	1.42	675M	800
EDM2-XXL (Karras et al., 2024)	63	1.91	1.5B	734	Light.DiT (Yao et al., 2025)	250×2	2.11	675M	64
DiT-XL/2 ⊕ DC-AE	250×2	2.41	675M	400	Light.DiT (Yao et al., 2025)	250×2	1.35	675M	800
GANs									
BigGAN (Brock et al., 2018)	1	8.43	160M	-	BigGAN (Brock et al., 2018)	1	6.95	112M	-
StyleGAN (Sauer et al., 2022)	1×2	2.41	168M	-	GigaGAN (Kang et al., 2023)	1	3.45	569M	-
Masked & autoregressive models									
MaskGIT (Chang et al., 2022)	12	7.32	227M	300	MaskGIT (Chang et al., 2022)	8	6.18	227M	300
VAR-d36-s (Tian et al., 2024)	10×2	2.63	2.3B	350	VAR-d30-re (Tian et al., 2024)	10×2	1.73	2.0B	350
Single-branch one-step models (distillation-based)									
sCD-M (Lu & Song, 2024)	1	2.75	498M	1997	UCGM-XL/2 (Sun et al., 2025)	1	2.10	675M	424
	2	2.26	498M	1997		2	1.94	675M	424
sCD-L (Lu & Song, 2024)	1	2.55	778M	1434	UCGM ⊕ REPA-XL/2	2	1.95	675M	801
	2	2.04	778M	1434	UCGM ⊕ Light.DiT	2	2.06	675M	801
sCD-XXL (Lu & Song, 2024)	1	2.28	1.5B	921	UCGM ⊕ DDT-XL/2	2	1.90	675M	401
	2	1.88	1.5B	921	π -Flow (Chen et al., 2025a)	1	3.34	675M	448
UCGM-XL (Sun et al., 2025)	1	2.63	675M	360	π -Flow ⊕ REPA-XL/2	1	2.85	675M	448
Single-branch one-step models (teacher-free)									
sCT-M (Lu & Song, 2024)	1	5.84	498M	1837	Shortcut-XL/2 (Frans et al., 2024)	1	10.6	676M	250
	2	5.53	498M	1837		4	7.80	676M	250
sCT-L (Lu & Song, 2024)	1	5.15	778M	1274	IMM-XL/2 (Zhou et al., 2025)	1×2	7.77	675M	3840
	2	4.65	778M	1274		2×2	5.33	675M	3840
sCT-XXL (Lu & Song, 2024)	1	4.29	1.5B	762	IMM-XL/2 ($\omega = 1.5$)	1×2	8.05	675M	3840
	2	3.76	1.5B	762		2×2	3.99	675M	3840
MeanFlow-XL/4 (Geng et al., 2025)	1	4.21	676M	360	MeanFlow-XL/2 (Geng et al., 2025)	1	3.43	676M	240
	2	3.41	676M	360		2	2.93	676M	240
MeanFlow-XL/2 ⊕ DC-AE	2	2.73	676M	840	MeanFlow-XL/2 (longer training)	2	2.20	676M	1000
Dual-branch one-step models (teacher-free)									
DuMo-XL/4	1	3.47	679M	360	DuMo-XL/2	1	3.07	679M	240
DuMo-XL/4	2	2.76	679M	360	DuMo-XL/2	2	2.82	679M	240
DuMo-XL/2 ⊕ DC-AE	1	2.89	679M	840	DuMo-XL/2 (longer training)	1	2.60	679M	432
DuMo-XL/2 ⊕ DC-AE	2	2.23	679M	840	DuMo-XL/2 (longer training)	2	1.79	679M	432

achieve further breakthroughs, we conjecture that future work must look beyond homologous ODE solvers and explore **heterogeneous** algorithms—such as adversarial learning (GANs)—that can provide orthogonal training signals.

4.4. Ablation Studies

To validate the effectiveness of our design choices, we conduct comprehensive ablation studies on ImageNet 256 × 256. We analyze three critical dimensions: the sensitivity to the loss weighting factor β , training computational efficiency, and the impact of time step sampling distributions. The results are summarized in Fig. 4.

Impact of velocity ratio (β). Fig. 4a reveals an advantage for our paradigm. DuMo (green stars) consistently outperforms the single-branch MeanFlow (blue circles) across the

majority of the spectrum, particularly in the effective convergence regimes. Crucially, DuMo achieves a significantly deeper basin of convergence (best FID=63.86) compared to the optimal MeanFlow (best FID=76.04).

This empirical observation aligns with our expectation of higher data efficiency: by leveraging unified supervision without strictly partitioning the budget, DuMo accelerates optimization. This also corroborates the findings in Tab. 1, explaining why our method yields superior performance under comparable or reduced training steps.

Training efficiency. A common concern is that dual-output architectures might incur significant computational overhead. However, Fig. 4b dispels this assumption. DuMo (purple bars) consistently demonstrates higher training throughput (Steps/Sec) compared to MeanFlow (blue bars)

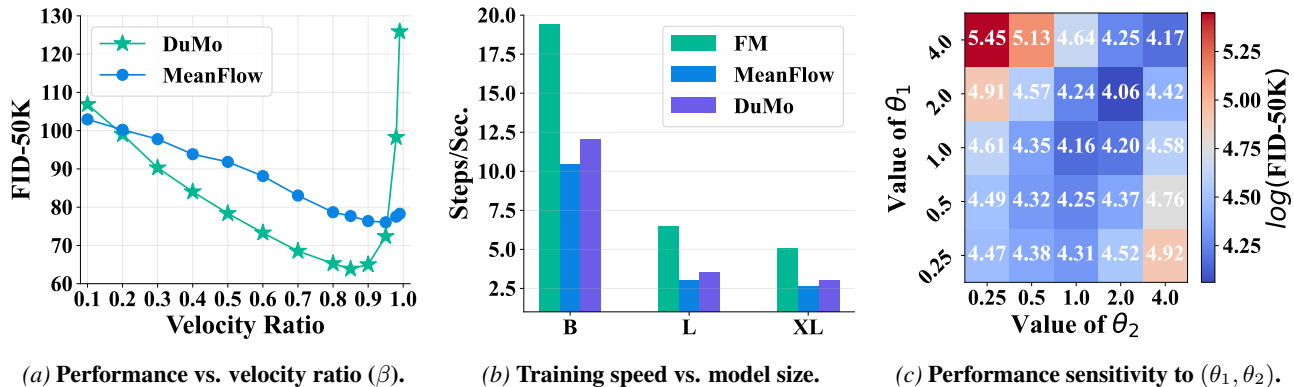


Figure 4. Ablation studies of DUMo on ImageNet-1K 256×256 . We investigate key design factors of DUMo for one-step generation, benchmarking against the single-branch baseline, MeanFlow. Unless noted otherwise, experiments in (a) and (c) employ a DiT-B/2 backbone trained for 10K iterations with a learning rate of 2×10^{-4} , adhering to the optimization protocol in Sec. 4.1.

across all model sizes (B, L, XL). Specifically, on the DiT-XL backbone, DUMo achieves a speedup of approximately 12.6%. This efficiency stems from the streamlined target construction described in Alg. 1: by reusing the stop-gradient velocity estimate $\mathbf{v}_{\theta,t}$, we reduce the per-step cost to just 1 gradient-based and 3 gradient-free forward passes (versus 4 for MeanFlow). Thus, DUMo balances advanced generative capabilities with computational economy.

Time distribution strategy. Fig. 4c presents a grid search over the Beta distribution parameters $t \sim \text{Beta}(\theta_1, \theta_2)$, measuring performance via $\log(\text{FID})$. We observe a clear “sweet spot” at $\theta_1 = 2.0, \theta_2 = 2.0$, which yields the lowest $\log(\text{FID})$ of 4.06 (deepest blue cell). This corresponds to a symmetric, bell-shaped distribution that concentrates sampling probability in the middle of the trajectory ($t \approx 0.5$). This finding suggests that the most critical signal for learning the consistency mapping lies in the intermediate noise regime, aligning with observations in prior literature (Sun et al., 2025; Rombach et al., 2022).

Comparison on CIFAR-10. Finally, we extend our evaluation to unconditional generation on CIFAR-10 (32×32) to benchmark against a broader range of methods. As detailed in Tab. 2, we compare DUMo against established few-step baselines including iCT (Song & Dhariwal, 2023), ECT (Geng et al., 2024), and IMM. All methods utilize the same U-Net backbone ($\sim 55\text{M}$ parameters) operating in pixel space. DUMo achieves an impressive one-step FID of 2.86. This result outperforms both the direct competitor MeanFlow (2.92) and sCT (2.97), and remains highly competitive with the SOTA iCT (2.83), demonstrating the robustness of our approach across different data modalities.

4.5. Additional Experiments and Analyses

Beyond the analysis in Sec. 4.4, we provide more details of the hyper-parameters used in our main experiments in

Table 2. System-level quality comparison for one-step generation task on unconditional CIFAR-10.

Method	iCT	ECT	sCT	IMM	MeanFlow	DUMo (ours)
NFE \downarrow	1	1	1	1	1	1
FID \downarrow	2.83	3.60	2.97	3.20	2.92	2.86

App. C.1. In addition to the standard metric (i.e., FID), we assess DUMo based on (a) qualitative visualization to demonstrate fine-grained details, and (b) the Inception Score (IS), another widely used metric for evaluating the fidelity of generated samples. Comprehensive results are in App. C.2.

Exploration of real-world applications. We validate the scalability of DUMo on two demanding tasks: text-to-image generation (App. C.3) and unified multimodal modeling (App. C.4). Notably, in text-to-image synthesis, DUMo establishes a new efficiency benchmark, achieving a GenEval score of 0.82 with just 2 NFE. This significantly surpasses the previous SOTA, SANA-Sprint (Chen et al., 2025b) (0.77), demonstrating superior performance in computationally constrained regimes.

5. Conclusion

In this work, we introduce **Duality Models** (DUMo), a unified framework that fundamentally resolves the “budget partition dilemma” inherent in target-aware generative models by embracing the core philosophy we term “**Let one Do More!**”: unifying distinct capabilities within a single representation. Specifically, by transitioning from a conditional “one input, one output” switch to a parallel “one input, dual output” paradigm, DUMo effectively leverages the PF-ODE velocity as a geometric regularizer for the flow-map integral. This architectural innovation enables a 679M parameter DiT to achieve SOTA performance (FID 1.79) on ImageNet 256×256 in just 2 steps, successfully bridging the stability of flow matching with the efficiency of consistency models without relying on pre-trained teachers.

Impact Statement

This paper introduces Duality Models, a framework designed to significantly accelerate the inference of diffusion probabilistic models while maintaining high generation quality. Our work has two primary societal implications:

Environmental and Accessibility Impact: By reducing the required sampling steps from hundreds to as few as one or two, our method substantially lowers the computational cost and energy consumption associated with generative model inference. This efficiency contributes to “Green AI” initiatives and helps democratize access to high-fidelity generation tools on consumer-grade hardware.

Potential for Misuse: As with any advancement in high-fidelity image synthesis, there is a risk that these techniques could be misused for creating misleading content or deep-fakes. While our focus is on the fundamental optimization of the generative process, we advocate for the responsible deployment of such models, including the integration of watermarking and provenance tracking technologies to mitigate malicious use.

References

- Bao, F., Nie, S., Xue, K., Cao, Y., Li, C., Su, H., and Zhu, J. All are worth words: A vit backbone for diffusion models. In *Proceedings of the IEEE/CVF conference on computer vision and pattern recognition*, pp. 22669–22679, 2023.
- Brock, A., Donahue, J., and Simonyan, K. Large scale gan training for high fidelity natural image synthesis. *arXiv preprint arXiv:1809.11096*, 2018.
- Chang, H., Zhang, H., Jiang, L., Liu, C., and Freeman, W. T. Maskgit: Masked generative image transformer. In *Proceedings of the IEEE/CVF conference on computer vision and pattern recognition*, pp. 11315–11325, 2022.
- Chen, H., Zhang, K., Tan, H., Guibas, L., Wetzstein, G., and Bi, S. pi-flow: Policy-based few-step generation via imitation distillation. *arXiv preprint arXiv:2510.14974*, 2025a.
- Chen, J., Cai, H., Chen, J., Xie, E., Yang, S., Tang, H., Li, M., Lu, Y., and Han, S. Deep compression autoencoder for efficient high-resolution diffusion models. *arXiv preprint arXiv:2410.10733*, 2024a.
- Chen, J., Wu, Y., Luo, S., Xie, E., Paul, S., Luo, P., Zhao, H., and Li, Z. Pixart- $\{\delta\}$: Fast and controllable image generation with latent consistency models. *arXiv preprint arXiv:2401.05252*, 2024b.
- Chen, J., Xue, S., Zhao, Y., Yu, J., Paul, S., Chen, J., Cai, H., Xie, E., and Han, S. Sana-sprint: One-step diffusion with continuous-time consistency distillation. *arXiv preprint arXiv:2503.09641*, 2025b.
- Cheng, Z., Sun, P., Li, J., and Lin, T. Twinflow: Realizing one-step generation on large models with self-adversarial flows. *arXiv preprint arXiv:2512.05150*, 2025.
- Dao, T., Fu, D., Ermon, S., Rudra, A., and Ré, C. Flashattention: Fast and memory-efficient exact attention with io-awareness. *Advances in neural information processing systems*, 35:16344–16359, 2022.
- Deng, J., Dong, W., Socher, R., Li, L.-J., Li, K., and Fei-Fei, L. Imagenet: A large-scale hierarchical image database. In *2009 IEEE conference on computer vision and pattern recognition*, pp. 248–255. Ieee, 2009.
- Dhariwal, P. and Nichol, A. Diffusion models beat gans on image synthesis. *Advances in neural information processing systems*, 34:8780–8794, 2021.
- Frans, K., Hafner, D., Levine, S., and Abbeel, P. One step diffusion via shortcut models. *arXiv preprint arXiv:2410.12557*, 2024.
- Geng, Z., Pokle, A., Luo, W., Lin, J., and Kolter, J. Z. Consistency models made easy. *arXiv preprint arXiv:2406.14548*, 2024.
- Geng, Z., Deng, M., Bai, X., Kolter, J. Z., and He, K. Mean flows for one-step generative modeling. *arXiv preprint arXiv:2505.13447*, 2025.
- Heusel, M., Ramsauer, H., Unterthiner, T., Nessler, B., and Hochreiter, S. Gans trained by a two time-scale update rule converge to a local nash equilibrium. *Advances in neural information processing systems*, 30, 2017.
- Ho, J. and Salimans, T. Classifier-free diffusion guidance. *arXiv preprint arXiv:2207.12598*, 2022.
- Ho, J., Jain, A., and Abbeel, P. Denoising diffusion probabilistic models. *Advances in neural information processing systems*, 33:6840–6851, 2020.
- Jiang, D., Liu, D., Wang, Z., Wu, Q., Li, L., Li, H., Jin, X., Liu, D., Li, Z., Zhang, B., et al. Distribution matching distillation meets reinforcement learning. *arXiv preprint arXiv:2511.13649*, 2025.
- Kang, M., Zhu, J.-Y., Zhang, R., Park, J., Shechtman, E., Paris, S., and Park, T. Scaling up gans for text-to-image synthesis. In *Proceedings of the IEEE/CVF conference on computer vision and pattern recognition*, pp. 10124–10134, 2023.
- Karras, T., Aittala, M., Aila, T., and Laine, S. Elucidating the design space of diffusion-based generative models. *Advances in neural information processing systems*, 35: 26565–26577, 2022.

- Karras, T., Aittala, M., Lehtinen, J., Hellsten, J., Aila, T., and Laine, S. Analyzing and improving the training dynamics of diffusion models. In *Proceedings of the IEEE/CVF Conference on Computer Vision and Pattern Recognition*, pp. 24174–24184, 2024.
- Kim, D., Lai, C.-H., Liao, W.-H., Murata, N., Takida, Y., Uesaka, T., He, Y., Mitsufuji, Y., and Ermon, S. Consistency trajectory models: Learning probability flow ode trajectory of diffusion. *arXiv preprint arXiv:2310.02279*, 2023.
- Labs, B. F. Flux. <https://github.com/black-forest-labs/flux>, 2024.
- Lin, S., Wang, A., and Yang, X. Sdxl-lightning: Progressive adversarial diffusion distillation. *arXiv preprint arXiv:2402.13929*, 2024.
- Lipman, Y., Chen, R. T., Ben-Hamu, H., Nickel, M., and Le, M. Flow matching for generative modeling. *arXiv preprint arXiv:2210.02747*, 2022.
- Liu, D., Gao, P., Liu, D., Du, R., Li, Z., Wu, Q., Jin, X., Cao, S., Zhang, S., Li, H., et al. Decoupled dmd: Cfg augmentation as the spear, distribution matching as the shield. *arXiv preprint arXiv:2511.22677*, 2025.
- Loshchilov, I. and Hutter, F. Decoupled weight decay regularization. *arXiv preprint arXiv:1711.05101*, 2017.
- Lu, C. and Song, Y. Simplifying, stabilizing and scaling continuous-time consistency models. *arXiv preprint arXiv:2410.11081*, 2024.
- Luhman, E. and Luhman, T. Knowledge distillation in iterative generative models for improved sampling speed. *ArXiv*, abs/2101.02388, 2021. URL <https://api.semanticscholar.org/CorpusID:230799531>.
- Luo, S., Tan, Y., Huang, L., Li, J., and Zhao, H. Latent consistency models: Synthesizing high-resolution images with few-step inference. *arXiv preprint arXiv:2310.04378*, 2023.
- Luo, T., Yuan, H., and Liu, Z. Soflow: Solution flow models for one-step generative modeling. *arXiv preprint arXiv:2512.15657*, 2025.
- Ma, N., Goldstein, M., Albergo, M. S., Boffi, N. M., Vanden-Eijnden, E., and Xie, S. Sit: Exploring flow and diffusion-based generative models with scalable interpolant transformers. In *European Conference on Computer Vision*, pp. 23–40. Springer, 2024.
- Nie, W., Berner, J., Ma, N., Liu, C., Xie, S., and Vahdat, A. Transition matching distillation for fast video generation. *arXiv preprint arXiv:2601.09881*, 2026.
- Paszke, A. Pytorch: An imperative style, high-performance deep learning library. *arXiv preprint arXiv:1912.01703*, 2019.
- Peebles, W. and Xie, S. Scalable diffusion models with transformers. In *Proceedings of the IEEE/CVF international conference on computer vision*, pp. 4195–4205, 2023.
- Peng, Y., Zhu, K., Liu, Y., Wu, P., Li, H., Sun, X., and Wu, F. Facm: Flow-anchored consistency models. *arXiv preprint arXiv:2507.03738*, 2025.
- Pu, Y., Han, Y., Tang, Z., Tang, J., Wang, F., Zhuang, B., and Huang, G. Few-step distillation for text-to-image generation: A practical guide. *arXiv preprint arXiv:2512.13006*, 2025.
- Rombach, R., Blattmann, A., Lorenz, D., Esser, P., and Ommer, B. High-resolution image synthesis with latent diffusion models. In *Proceedings of the IEEE/CVF conference on computer vision and pattern recognition*, pp. 10684–10695, 2022.
- Salimans, T. and Ho, J. Progressive distillation for fast sampling of diffusion models. *arXiv preprint arXiv:2202.00512*, 2022.
- Salimans, T., Goodfellow, I., Zaremba, W., Cheung, V., Radford, A., and Chen, X. Improved techniques for training gans. *Advances in neural information processing systems*, 29, 2016.
- Sauer, A., Schwarz, K., and Geiger, A. Stylegan-xl: Scaling stylegan to large diverse datasets. In *ACM SIGGRAPH 2022 conference proceedings*, pp. 1–10, 2022.
- Sauer, A., Boesel, F., Dockhorn, T., Blattmann, A., Esser, P., and Rombach, R. Fast high-resolution image synthesis with latent adversarial diffusion distillation. In *SIGGRAPH Asia 2024 Conference Papers*, pp. 1–11, 2024a.
- Sauer, A., Lorenz, D., Blattmann, A., and Rombach, R. Adversarial diffusion distillation. In *European Conference on Computer Vision*, pp. 87–103. Springer, 2024b.
- Song, Y. and Dhariwal, P. Improved techniques for training consistency models. *arXiv preprint arXiv:2310.14189*, 2023.
- Song, Y., Sohl-Dickstein, J., Kingma, D. P., Kumar, A., Ermon, S., and Poole, B. Score-based generative modeling through stochastic differential equations. *arXiv preprint arXiv:2011.13456*, 2020.
- Song, Y., Dhariwal, P., Chen, M., and Sutskever, I. Consistency models. *arXiv preprint arXiv:2303.01469*, 2023.

- Sun, P. and Lin, T. Any-step generation via n-th order recursive consistent velocity field estimation. In *The Fourteenth International Conference on Learning Representations*, 2026. URL <https://openreview.net/forum?id=GnawtLKGkP>.
- Sun, P., Jiang, Y., and Lin, T. Unified continuous generative models. *arXiv preprint arXiv:2505.07447*, 2025.
- Team, T. H. Hunyuanimage 2.1: An efficient diffusion model for high-resolution (2k) text-to-image generation. <https://github.com/Tencent-Hunyuan/HunyuanImage-2.1>, 2025.
- Tian, K., Jiang, Y., Yuan, Z., Peng, B., and Wang, L. Visual autoregressive modeling: Scalable image generation via next-scale prediction. *Advances in neural information processing systems*, 37:84839–84865, 2024.
- Tong, S., Ma, N., Xie, S., and Jaakkola, T. Flow map distillation without data. *arXiv preprint arXiv:2511.19428*, 2025.
- Wang, S., Tian, Z., Huang, W., and Wang, L. Ddt: Decoupled diffusion transformer. *arXiv preprint arXiv:2504.05741*, 2025.
- Wu, C., Li, J., Zhou, J., Lin, J., Gao, K., Yan, K., ming Yin, S., Bai, S., Xu, X., Chen, Y., Chen, Y., Tang, Z., Zhang, Z., Wang, Z., Yang, A., Yu, B., Cheng, C., Liu, D., Li, D., Zhang, H., Meng, H., Wei, H., Ni, J., Chen, K., Cao, K., Peng, L., Qu, L., Wu, M., Wang, P., Yu, S., Wen, T., Feng, W., Xu, X., Wang, Y., Zhang, Y., Zhu, Y., Wu, Y., Cai, Y., and Liu, Z. Qwen-image technical report, 2025a. URL <https://arxiv.org/abs/2508.02324>.
- Wu, S., Wu, Z., Gong, Z., Tao, Q., Jin, S., Li, Q., Li, W., and Loy, C. C. Openuni: A simple baseline for unified multimodal understanding and generation. 2025b. URL <https://arxiv.org/abs/2505.23661>.
- Yao, J., Yang, B., and Wang, X. Reconstruction vs. generation: Taming optimization dilemma in latent diffusion models. *arXiv preprint arXiv:2501.01423*, 2025.
- Yin, T., Gharbi, M., Park, T., Zhang, R., Shechtman, E., Durand, F., and Freeman, W. T. Improved distribution matching distillation for fast image synthesis. *arXiv preprint arXiv:2405.14867*, 2024a.
- Yin, T., Gharbi, M., Zhang, R., Shechtman, E., Durand, F., Freeman, W. T., and Park, T. One-step diffusion with distribution matching distillation. In *Proceedings of the IEEE/CVF conference on computer vision and pattern recognition*, pp. 6613–6623, 2024b.
- Yu, S., Kwak, S., Jang, H., Jeong, J., Huang, J., Shin, J., and Xie, S. Representation alignment for generation: Training diffusion transformers is easier than you think. *arXiv preprint arXiv:2410.06940*, 2024.
- Yu, X., Qi, X., Li, Z., Zhang, K., Zhang, R., Lin, Z., Shechtman, E., Wang, T., and Nitzan, Y. Self-evaluation unlocks any-step text-to-image generation. *arXiv preprint arXiv:2512.22374*, 2025.
- Zhao, Y., Gu, A., Varma, R., Luo, L., Huang, C.-C., Xu, M., Wright, L., Shojanazeri, H., Ott, M., Shleifer, S., et al. Pytorch fsdp: experiences on scaling fully sharded data parallel. *arXiv preprint arXiv:2304.11277*, 2023.
- Zheng, H., Nie, W., Vahdat, A., and Anandkumar, A. Fast training of diffusion models with masked transformers. *arXiv preprint arXiv:2306.09305*, 2023.
- Zheng, K., Chen, Y., Chen, H., He, G., Liu, M.-Y., Zhu, J., and Zhang, Q. Direct discriminative optimization: Your likelihood-based visual generative model is secretly a gan discriminator. *arXiv preprint arXiv:2503.01103*, 2025a.
- Zheng, K., Wang, Y., Ma, Q., Chen, H., Zhang, J., Balaji, Y., Chen, J., Liu, M.-Y., Zhu, J., and Zhang, Q. Large scale diffusion distillation via score-regularized continuous-time consistency. *arXiv preprint arXiv:2510.08431*, 2025b.
- Zhou, L., Ermon, S., and Song, J. Inductive moment matching. *arXiv preprint arXiv:2503.07565*, 2025.

A. Limitations and Future Work

Despite these advancements, our current exploration is primarily limited to dual-branch systems involving homologous PF-ODE objectives. While preliminary experiments suggest that simply stacking additional ODE-based heads (e.g., shortcut or MeanFlow) yields diminishing returns due to signal redundancy, the broader potential of DUMO lies in its ability to fuse distinct generative paradigms. A critical and unexplored avenue is the integration of *heterogeneous* objectives. For instance, combining the geometric stability of flow matching with the perceptual sharpness of adversarial learning (GANs) or the statistical alignment of distribution matching losses (e.g., DMD (Yin et al., 2024b) or TwinFlow (Cheng et al., 2025)) could provide orthogonal training signals. We believe DUMO serves as a foundational blueprint for such unified, multi-objective architectures, opening new possibilities for pushing the boundaries of one-step generation quality.

B. Related Work

The landscape of continuous-time generative models has evolved from multi-step integration towards high-fidelity, few-step synthesis. Our work builds upon this trajectory by addressing the limitations of existing paradigms. We contextualize our contributions by surveying three dominant research thrusts—multi-step foundations, interval-based consistency, and adversarial refinement—and concluding with their specific challenges in large-scale applications.

B.1. Foundations: Multi-Step Integration of Instantaneous Fields

The dominant paradigm in continuous generative modeling, including Denoising Diffusion Models (Ho et al., 2020; Song et al., 2020; Dhariwal & Nichol, 2021) and Flow-Matching (Lipman et al., 2022), relies on learning an *instantaneous* velocity field. These models train a neural network to approximate the local dynamics $\frac{dx_t}{dt}$ of a Probability Flow Ordinary Differential Equation (PF-ODE). To generate a sample, one must numerically integrate this field, typically requiring hundreds or thousands of steps to ensure fidelity. The core limitation of this approach is its sensitivity to coarse discretization; when using few steps, large truncation errors accumulate, particularly for trajectories with high curvature, leading to a significant degradation in sample quality (Karras et al., 2022). This challenge has catalyzed the development of methods designed specifically for the few-step regime.

B.2. Interval-Based Consistency for Few-Step Generation

A major research thrust aims to overcome the integration bottleneck by enforcing consistency over finite time intervals or distilling the trajectory. Early distillation methods (Luhman & Luhman, 2021; Salimans & Ho, 2022) trained students to match teacher steps. Consistency Models (CMs) (Song et al., 2023; Song & Dhariwal, 2023) advanced this by enforcing a *relative* constraint: the model’s prediction of the trajectory’s endpoint (x_0) should be consistent across different starting points. This concept was extended by methods like MeanFlow (Geng et al., 2025), which directly models the average velocity.

Improving Training Efficiency and Objectives. A critical implementation challenge is the efficient computation of time derivatives. Early methods relied on Jacobian-Vector Products (JVP) (Geng et al., 2025; Lu & Song, 2024), which are computationally intensive and incompatible with modern optimizations like FlashAttention (Dao et al., 2022) and FSDP (Zhao et al., 2023). Recent work addresses this bottleneck: Sun et al. (2025) propose finite-difference estimators, while SoFlow (Luo et al., 2025) introduces a solution consistency loss that bypasses JVP entirely. Similarly, T2I-Distill (Pu et al., 2025) develops efficient kernels for open-domain generation. New approaches continue to emerge: FACM (Peng et al., 2025) stabilizes training by anchoring to the instantaneous field, π -Flow (Chen et al., 2025a) adopts an imitation learning perspective, and Self-E (Yu et al., 2025) leverages self-evaluation to refine generation.

B.3. Adversarial and Distribution-Matching Refinement

A parallel approach achieves high-fidelity, one-step generation by incorporating external signals—either adversarial or distribution-matching—to explicitly anchor outputs to the data manifold. Methods such as CTM (Kim et al., 2023), ADD/LADD (Sauer et al., 2024b;a), and distillation techniques like DMD/DMD2 (Yin et al., 2024b;a) employ auxiliary discriminators or minimizing KL divergence to sharpen model outputs. Notably, recent works like TwinFlow (Cheng et al., 2025) further advance this direction by coupling dual flows to enforce distribution consistency without relying heavily on unstable adversarial min-max games. Other GAN-based refiners (Zheng et al., 2025a) similarly push the student to surpass

the teacher.

Recent advancements refine this paradigm: Decoupled-DMD (Liu et al., 2025) identifies CFG as the primary acceleration driver, while DMD-R (Jiang et al., 2025) integrates reinforcement learning for better mode coverage. However, this reliance is a double-edged sword. Adversarial and distribution-matching frameworks typically depend on a frozen, pre-trained teacher to generate synthetic data, the cost of which can be prohibitive for ultra-large models (Yin et al., 2024a). Moreover, auxiliary networks increase memory overhead and training instability. Approaches like Tong et al. (2025) attempt to mitigate this via data-free distillation from prior distributions, but balancing fidelity and complexity remains a key challenge.

B.4. Applications in Large-Scale Generative Models

The tension between speed and quality is amplified in state-of-the-art large-scale systems. For instance, Qwen-Image-20B (Wu et al., 2025a) typically requires 100 NFEs, resulting in substantial latency (~ 40 s for a 1024×1024 image on a single A100). While pipelines like Hunyuan-Image-2.1 (Team, 2025) have explored MeanFlow for mid-step acceleration, and others apply LCM-style or hybrid distillation (e.g., PixArt-Delta (Chen et al., 2024b), SDXL (Lin et al., 2024), FLUX-schnell (Labs, 2024), SANA-Sprint (Chen et al., 2025b), LCM (Luo et al., 2023)), targeting extreme acceleration (1-2 NFEs) for 10B-20B backbones remains difficult. The prohibitive memory costs of teacher-dependent pipelines and the instability of adversarial training hinder straightforward scaling. Beyond static images, this challenge extends to video generation, where recent works like rCM (Zheng et al., 2025b) and TMD (Nie et al., 2026) represent initial steps towards applying continuous-time consistency and decoupled distillation to temporally complex data.

C. Detailed Experiment

C.1. Implementation Details

Training setup. We implement all models using PyTorch and train them on NVIDIA GPUs. We employ the AdamW optimizer (Loshchilov & Hutter, 2017) with a global batch size of 512. The learning rate follows a constant schedule throughout training, with no warmup phase. To stabilize sampling, we apply Exponential Moving Average (EMA) to the model parameters with a decay rate of 0.9999.

Hyperparameter configuration. Detailed hyperparameter settings for ImageNet-1K training are provided in Tab. 3. Regarding the specific coefficients for DUMO: the Beta distribution parameters (θ_1, θ_2) determine the shape of the time sampling distribution during training (illustrated in Fig. 4c); the parameter β modulates the velocity ratio, representing the weight of the multi-step loss (see Fig. 4a); and ζ governs the scale of the training-time classifier-free guidance, following Sun et al. (2025).

Table 3. **Hyperparameter configurations for DUMO on ImageNet-1K.** This table details the settings for few-step training and sampling across different resolutions and architectures.

Task		Optimizer				DUMo			
Resolution	VAE/AE	Model	Type	lr	(β_1, β_2)	Transport	(θ_1, θ_2) (see Fig. 4c)	β (see Fig. 4a)	ζ (see Sun et al. (2025))
Few-step model training and sampling									
256	SD-VAE	XL/2	AdamW	0.0001	(0.9,0.95)	Linear	(2.4,2.4)	0.7	0.55
512	DC-AE	XL/1	AdamW	0.0001	(0.9,0.95)	Linear	(1.0,1.0)	0.7	0.66
	SD-VAE	XL/4	AdamW	0.0001	(0.9,0.95)	Linear	(2.4,2.4)	0.7	0.66

C.2. Additional Results on ImageNet-1K

In this section, we provide a comprehensive evaluation of generation quality on ImageNet-1K (256×256), complementing the main results in Sec. 4. Beyond the standard Fréchet Inception Distance (FID), we report the Inception Score (IS) (Salimans et al., 2016) to explicitly assess the diversity and class-conditional distinctiveness of the generated samples. We compare our proposed DUMO against the strongest single-branch baseline, MeanFlow (Geng et al., 2025), under identical training budgets (432 epochs).

Quantitative analysis. As illustrated in Fig. 7 through Fig. 10, DUMO consistently outperforms MeanFlow across both sampling regimes.

- (a) **One-step Generation:** At 1 NFE, DUMO achieves an IS of **246.26** and an FID of **2.60**, surpassing MeanFlow (IS 239.58, FID 2.87). This confirms that our dual-branch design effectively mitigates the “starvation” of the generative head, allowing for better convergence even in the ultra-low step regime.
- (b) **Two-step Generation:** The performance gap widens significantly when a second denoising step is allowed. DUMO achieves a remarkable IS of **285.67** and an SOTA FID of **1.79** (Fig. 10). In contrast, MeanFlow saturates at an IS of 254.39 and FID of 2.39 (Fig. 9). The substantially higher Inception Score (+31.28 points) indicates that our model captures a much richer diversity of ImageNet classes with higher confidence, validating the efficacy of the velocity-guided regularization.

Qualitative analysis. We provide randomly sampled visualizations to corroborate these metrics. Fig. 7 and Fig. 9 show samples from MeanFlow. While structurally coherent, they occasionally exhibit texture over-smoothing or minor artifacts in complex geometries. In comparison, samples from DUMO (Fig. 8 and Fig. 10) demonstrate superior perceptual fidelity. Notably, in the 2-step regime, our model generates images with sharp fine-grained details and accurate semantic structures, closely approximating the data distribution. This visual evidence aligns with our hypothesis: by simultaneously enforcing local geometric constraints (velocity) and global consistency (flow-map) on every sample, DUMO learns a more robust and accurate transport trajectory.

C.3. Comparison with Text-to-image Models

To investigate the versatility of the DUMO paradigm beyond the scope of standard class-conditional generation, we extend our evaluation to the more challenging text-to-image synthesis task. This benchmark serves to verify whether the architectural advantages of our dual-branch design can effectively translate to open-domain scenarios involving complex semantic control. Comprehensive experimental analyses and qualitative comparisons will be presented in the forthcoming version of this manuscript.

C.4. Experimental Results on Large-scale Unified Multimodal Models

To rigorously assess the robustness and scalability of DUMO under regimes of extreme parameter counts, we further evaluate our framework within the domain of Unified Multimodal Models (UMMs). We benchmark our approach against state-of-the-art large-scale foundational models, such as Qwen-Image-20B (Wu et al., 2025a) and OpenUni (Wu et al., 2025b), to validate the efficacy of the proposed objective at scale. The detailed quantitative results from this large-scale evaluation will be updated in the future manuscript.

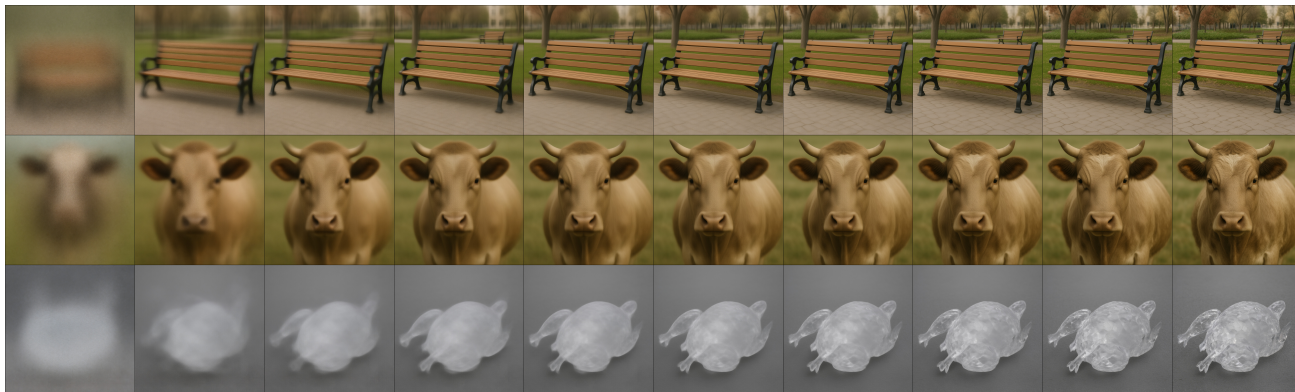


Figure 5. **Visualization of sampling trajectories at the baseline state (0 training steps).** Initially, the model requires significant computational steps to resolve coherent images. The leftmost columns (low NFE) remain unstructured and blurry, with high-fidelity results only emerging in the rightmost columns, indicating a highly curved generation trajectory typical of the teacher model.

Qualitative analysis of convergence trend. To explicitly verify the convergence trend of the model towards a few-step generator, we compare the visualization of sampling trajectories at different training stages. As shown in Fig. 5 (0 steps), the initial model follows the teacher’s curved trajectory, where coherent image structure only emerges at higher NFEs (right columns), with low-NFE outputs remaining largely unstructured. Conversely, Fig. 6 (3000 steps) clearly demonstrates the model is converging: even at the lowest NFEs (leftmost columns), the generated images—such as the park bench, cow, and crystal chicken—already exhibit clear structures and recognizable details, representing a significant improvement over

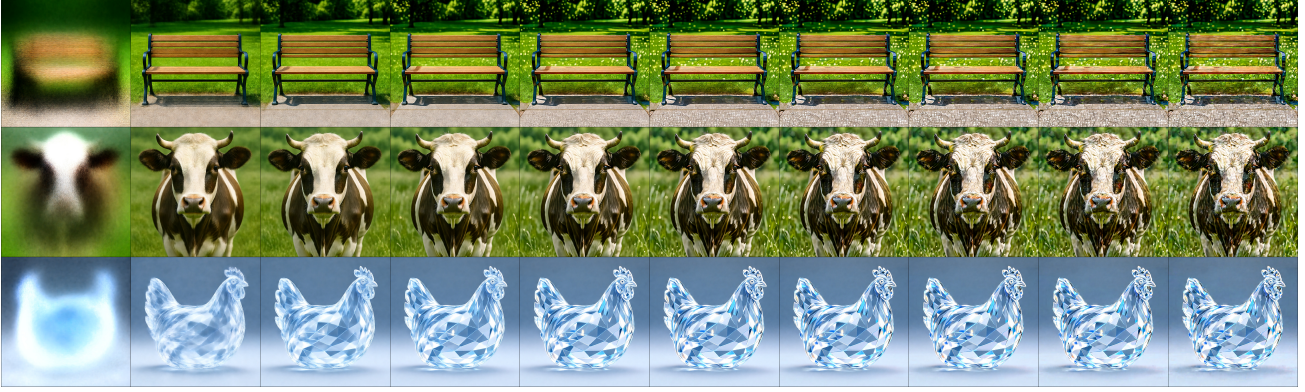


Figure 6. **Visualization of sampling trajectories demonstrating the trend towards convergence (3000 training steps).** At this intermediate training stage, DUMO already shows significant improvement in few-step generation. Compared to Fig. 5, clear object structures emerge much earlier at lower NFEs (left columns), visually affirming that the generation trajectory is being effectively straightened towards a few-step model.

the initial state. This visual evidence confirms that DUMO is effectively straightening the generation flow, progressively enabling the model to map noise to high-quality data in fewer steps.

D. Theoretical Analysis

Intrinsic encompassment of multi-step dynamics in consistency learning. To understand the theoretical legitimacy of the proposed DUMO, we analyze the composition of the consistency training objective. Following the unified perspective established in Sun et al. (2025), we demonstrate that the learning target of one-step consistency models inherently encompasses the objective of multi-step flow matching.

Theorem 1 (Surrogate objective for unified linear case ($\alpha(t) = t$, $\gamma(t) = 1 - t$), see Sun et al. (2025)). *The training of consistency-based models can be analyzed via a surrogate loss function $\mathcal{L}(\theta, \lambda)$. Here, $\lambda \in (0, 1)$ denotes the **Consistency Ratio**. This objective asymptotically recovers flow matching models as $\lambda \rightarrow 0$ and approximates consistency models as $\lambda \rightarrow 1$. Crucially, for any λ , the objective decomposes as:*

$$\mathcal{L}(\theta, \lambda) = \mathbb{E}_{\mathbf{z}, \mathbf{x}, t} \left[\underbrace{\|\mathbf{F}_{\theta}(\mathbf{x}_t, t) - \mathbf{z}_t\|_2^2}_{\text{Flow Matching Term}} + \frac{\lambda}{1 - \lambda} \underbrace{\|\mathbf{F}_{\theta}(\mathbf{x}_t, t) - \mathbf{F}_{\theta^-}(\mathbf{x}_{\lambda t}, \lambda t)\|_2^2}_{\text{Self-Alignment Term}} \right], \quad (10)$$

where $\mathbf{x}_t = t \cdot \mathbf{z} + (1 - t) \cdot \mathbf{x}$ and $\mathbf{z}_t = \mathbf{z} - \mathbf{x}$.

Thm. 1 provides two critical insights that justify the DUMO paradigm:

Gradient compatibility. (10) reveals that the standard consistency objective is effectively a superposition of a velocity regression loss (first term) and a self-alignment loss (second term). Consequently, the gradient direction derived from consistency training *already contains* the gradient component required for flow matching. This theoretical inclusion implies that explicitly adding a flow matching loss via a secondary head (as done in DUMO) does not introduce adversarial gradients or objective conflicts. Instead, it acts as a **compatible reinforcement**, explicitly supervising a signal that the consistency objective was already implicitly attempting to minimize.

Implicit-to-explicit duality. Since the flow matching term is an intrinsic component of the surrogate objective, a well-trained one-step consistency model must, by definition, implicitly capture the multi-step velocity field to achieve minimal loss. In other words, a functional one-step generator naturally contains a multi-step estimator within its latent representations. Therefore, the design of DUMO—extracting this implicit knowledge via a dedicated velocity head—is a natural architectural evolution. It allows the shared backbone to learn a unified representation that is valid for both local differential dynamics (\mathbf{v}_t) and global integral mappings (\mathbf{u}_t) without representation collapse or task interference.

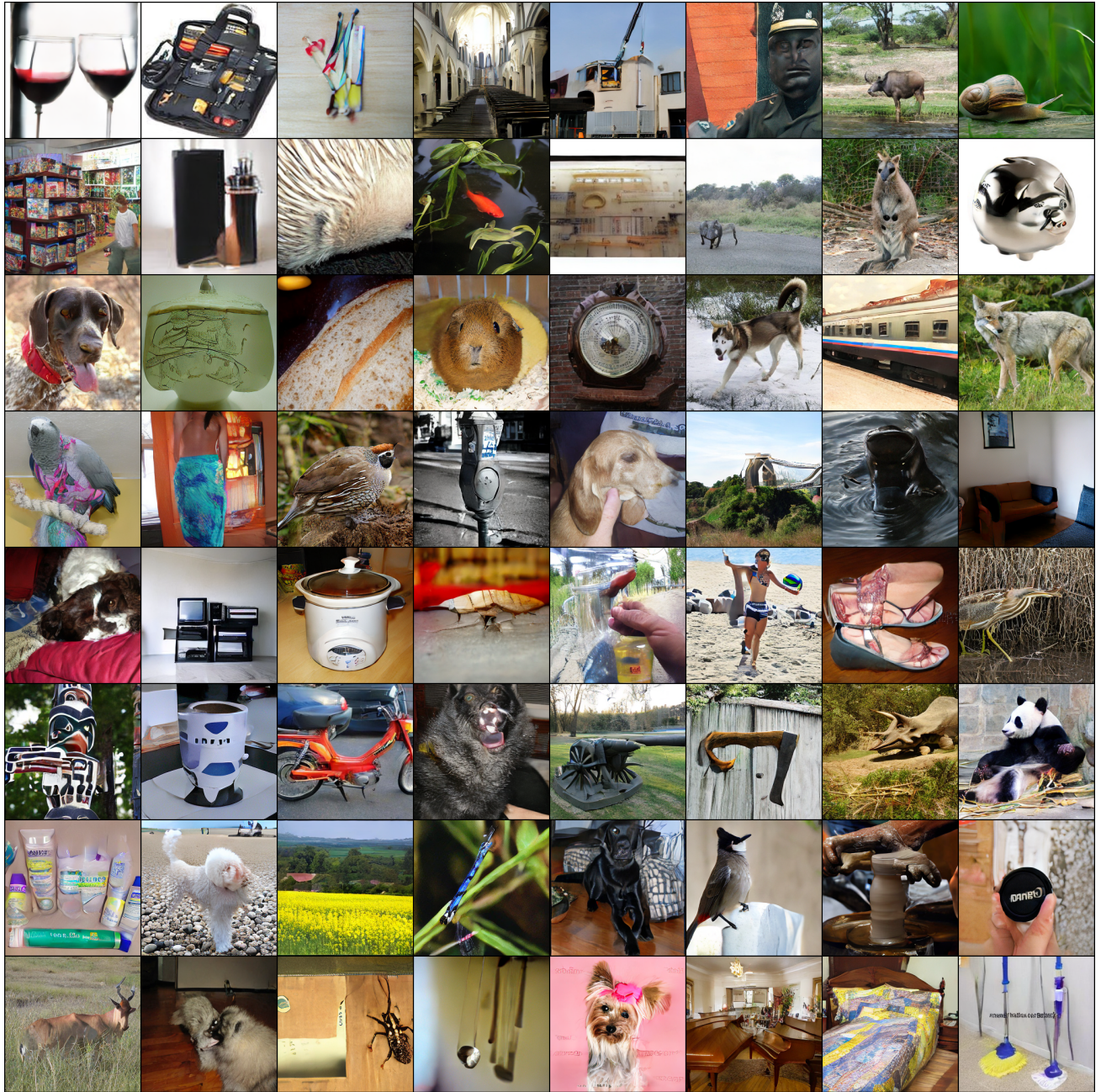


Figure 8. Visualization of randomly generated images (256×256) from our DuMO-XL/2. The model was trained for 432 epochs and sampled using 1 NFE, achieving FID= 2.60 and IS= 246.26.

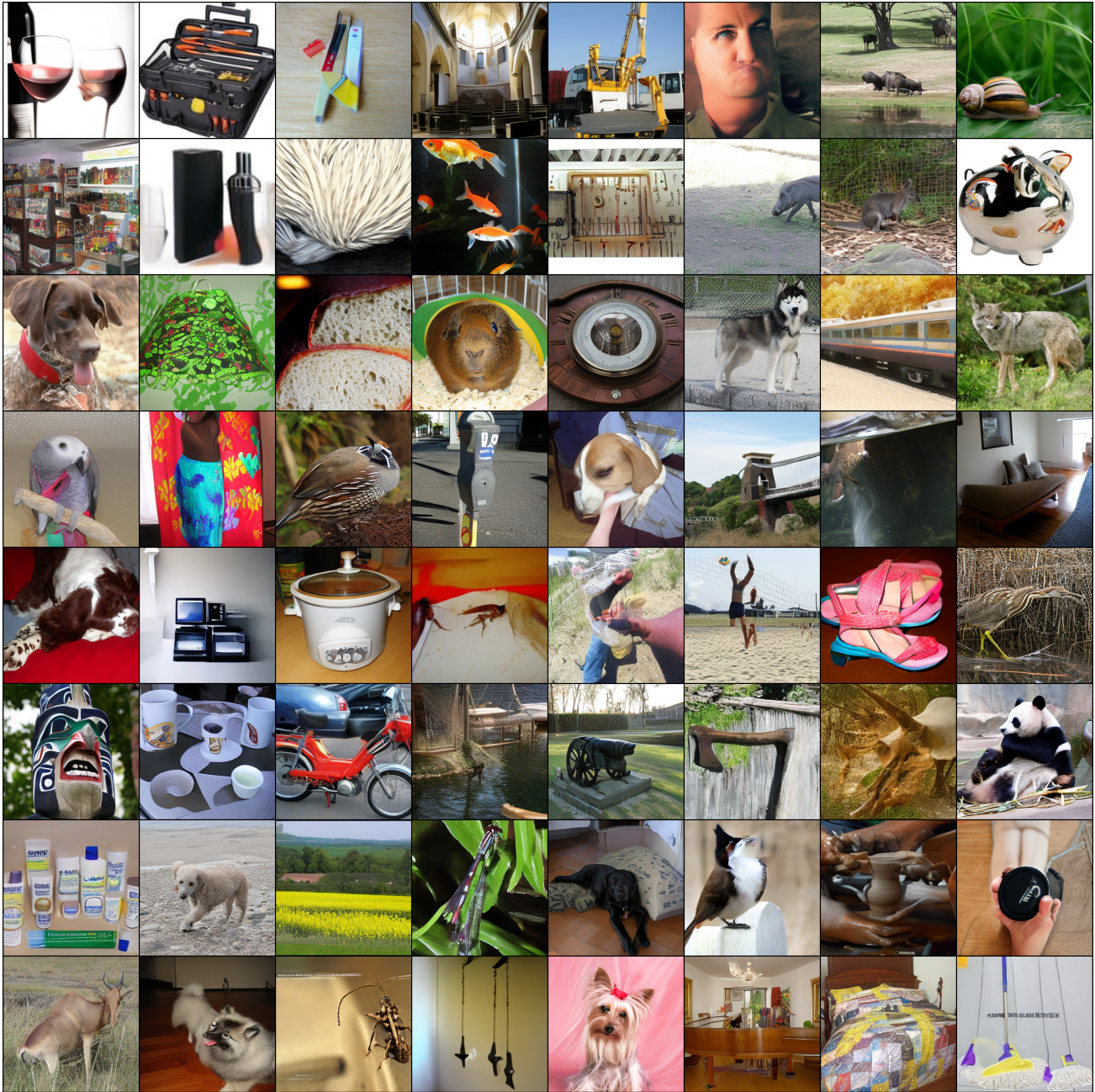


Figure 9. Visualization of randomly generated images (256×256) from MeanFlow-XL/2 (Geng et al., 2025). The model was trained for 432 epochs and sampled using 2 NFE, achieving FID= 2.39 and IS= 254.39.

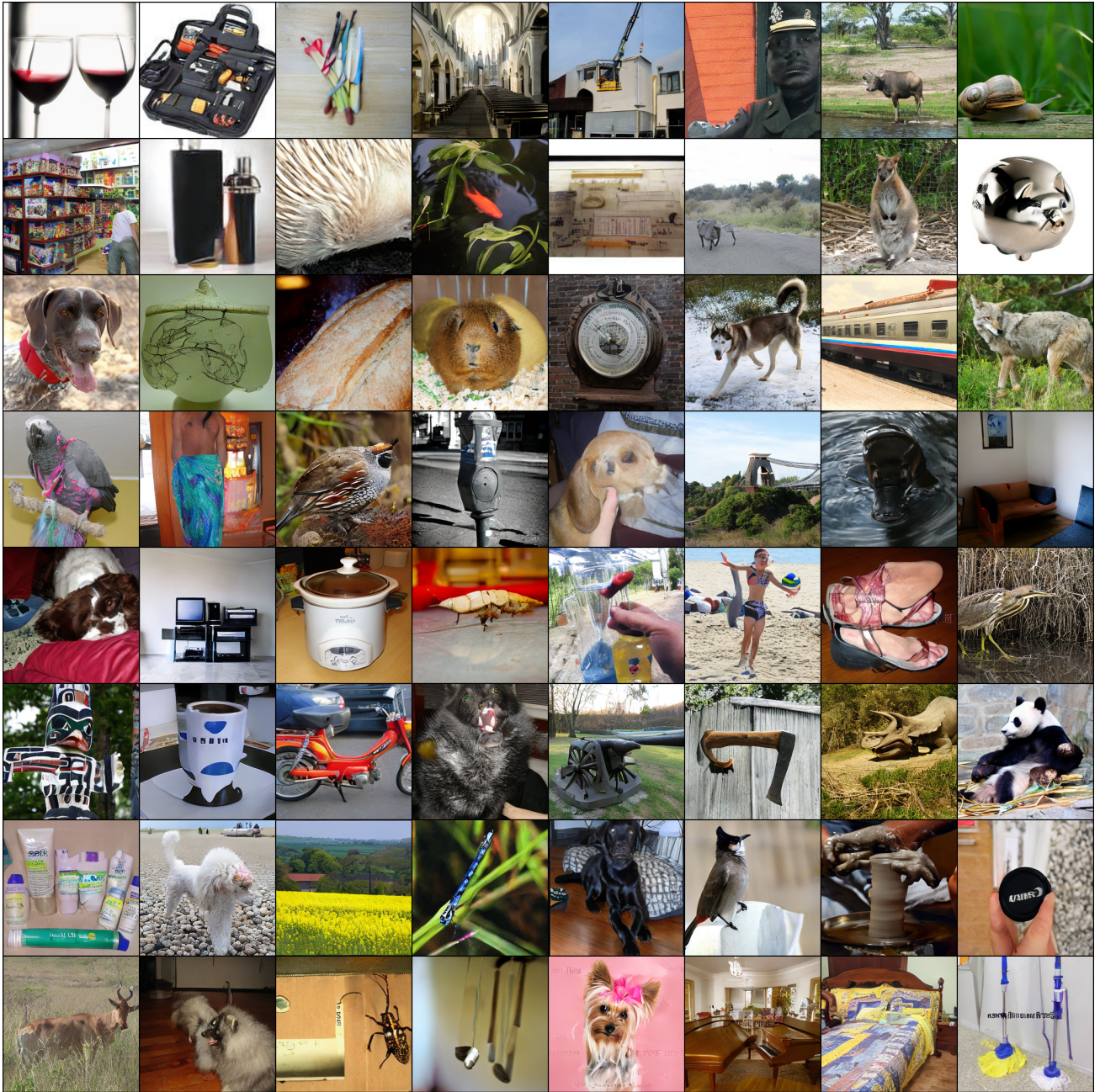


Figure 10. Visualization of randomly generated images (256×256) from our DuMO-XL/2. The model was trained for 432 epochs and sampled using 2 NFE, achieving FID= 1.79 and IS= 285.67.